



**HAL**  
open science

## High-speed photography during ultrasound illustrates potential therapeutic applications of microbubbles

Michiel Postema, Annemieke van Wamel, Folkert J. ten Cate, Nico de Jong

► **To cite this version:**

Michiel Postema, Annemieke van Wamel, Folkert J. ten Cate, Nico de Jong. High-speed photography during ultrasound illustrates potential therapeutic applications of microbubbles. *Medical Physics*, 2005, 32 (12), pp.3707-3711. 10.1118/1.2133718 . hal-03193350

**HAL Id: hal-03193350**

**<https://hal.science/hal-03193350>**

Submitted on 11 Apr 2021

**HAL** is a multi-disciplinary open access archive for the deposit and dissemination of scientific research documents, whether they are published or not. The documents may come from teaching and research institutions in France or abroad, or from public or private research centers.

L'archive ouverte pluridisciplinaire **HAL**, est destinée au dépôt et à la diffusion de documents scientifiques de niveau recherche, publiés ou non, émanant des établissements d'enseignement et de recherche français ou étrangers, des laboratoires publics ou privés.

# High-speed photography during ultrasound illustrates potential therapeutic applications of microbubbles

Michiel Postema<sup>¶</sup>, Annemieke van Wamel<sup>\*†</sup>, Folkert J. ten Cate<sup>#</sup>,  
Nico de Jong<sup>\*†‡</sup>

<sup>¶</sup> Institute for Medical Engineering, Ruhr-Universität Bochum, Bochum, Germany;

<sup>\*</sup> Dept. of Experimental Echocardiography, Thoraxcentre, Erasmus MC, Rotterdam, The Netherlands;

<sup>#</sup> Dept. of Cardiology, Thoraxcentre, Erasmus MC, Rotterdam, The Netherlands;

<sup>†</sup> Interuniversity Cardiology Institute of The Netherlands, Utrecht, The Netherlands;

<sup>‡</sup> Physics of Fluids Group, Faculty of Science and Technology, University of Twente, Enschede,  
The Netherlands

Corresponding author:

Dr. Michiel Postema

Institute for Medical Engineering

Ruhr-Universität Bochum

Building IC, 6/146

D-44780 Bochum

Germany

Tel: +49.234.3227740,

Fax: +49.234.3214872,

E-mail: [michiel.postema@rub.de](mailto:michiel.postema@rub.de)

Running title: Ultrasonic microbubbles for therapy

# High-speed photography during ultrasound illustrates potential therapeutic applications of microbubbles

## Abstract

Ultrasound contrast agents consist of microscopically small encapsulated bubbles that oscillate upon insonification. To enhance diagnostic ultrasound imaging techniques and to explore therapeutic applications, these medical microbubbles have been studied with the aid of high-speed photography. We filmed medical microbubbles at higher frame rates than the ultrasonic frequency transmitted. Microbubbles with thin lipid shells have been observed to act as microsyringes during one single ultrasonic cycle. This jetting phenomenon presumably causes sonoporation. Furthermore, we observed that the gas content can be forced out of albumin-encapsulated microbubbles. These free bubbles have been observed to jet, too. It is concluded that microbubbles might act as a vehicle to carry a drug in gas phase to a region of interest, where it has to be released by diagnostic ultrasound. This opens up a whole new area of potential applications of diagnostic ultrasound related to targeted imaging and therapeutic delivery of drugs such as nitric oxide.

## Technical Note

Ultrasound contrast agents consist of microscopically small encapsulated bubbles that oscillate upon insonification. Owing to their characteristic acoustic response, these medical microbubbles are becoming widespread in contemporary cardiology and radiology.<sup>1-4</sup> Ultrasound contrast agents have also been under investigation for therapeutic applications.<sup>5-7</sup> Since the acoustic interrogation of an agent takes place on an ensemble of microbubbles, the contribution of an individual microbubble to the acoustic response cannot be predicted. Therefore, the development of more sophisticated detection techniques, and the research on therapeutic

applications of medical microbubbles have to be based on other investigation methods, such as high-speed optical imaging.

We may define high-speed photography as the capturing of events that are more rapid than the human brain can process as a separate event, approximately  $1/15^{\text{th}}$  of a second. Its development started with Talbot's experiment in 1851.<sup>8</sup> He took a sharp picture of a newspaper rotating on a wheel, making use of spark illumination for about  $1/2,000^{\text{th}}$  of a second. The first multi-frame recording was done by Muybridge in 1878. He captured a sequence of 12 photographs of a trotting horse. Exposure times were 2 ms and interframe times 40 ms. Over the next years photographic technology rapidly improved, stimulated by the development of cinematography. Early applications of high-speed photography were mainly in ballistics.<sup>9,10</sup> Worthington was the first to investigate fluid dynamics by means of high-speed photography.<sup>11</sup> An elaborate overview of the development of high-speed photography in the nineteenth and twentieth century is given by Fuller and Rendell.<sup>12</sup> Nowadays, high-speed cameras capable of taking multiple frames are equipped with either beam splitters that divide an image over several recording devices, or a rotating mirror sweeping the image over numerous recording devices. Although recording speeds of 200 million frames per second can be reached with the former camera type, the total number of frames available is currently 16. With the latter technology, recording speeds of 25 million frames per second can be reached, whereas the total number of frames is virtually unlimited.

Over the past years, various attempts have been made to visualize the behavior of medical microbubbles during ultrasound irradiation. Klibanov *et al.* observed oscillations of ultrasound contrast agent microbubbles attached to a Petri dish with a 30 frames per second camera.<sup>13</sup> Dayton *et al.* combined acoustical observations of ultrasound contrast agent and optical observations with a 600 frames per second camera.<sup>14,15</sup> They observed gas release and bubble destruction. Takeuchi used TV-frame synchronous illumination and insonification to observe microballoon breakage.<sup>16,17</sup> Because of the low frame rates of the cameras mentioned, the

instance of shell breakage and the behavior of a bubble within an ultrasound cycle could not be observed. Only recently, observations of shell disruption and gas release within one ultrasonic cycle have been presented.<sup>18,19</sup> Kuribayashi *et al.* observed changes in ultrasound contrast agent microbubble diameters within one cycle of ultrasound, at frame rates up to 10 MHz and 50× magnification.<sup>20</sup> They concluded that the imaging frame rate and magnification were not sufficient for studying the details of ultrasound contrast agent bubble behavior. De Jong *et al.* carried out a preliminary study on this subject.<sup>21</sup> They proposed a method to visualize the oscillations of bubbles using a microscope and a fast framing camera operating at a 4 MHz frame rate. Furthermore, they compared radius–time curves, derived from two-dimensional bubble pictures, to a theoretical model. Morgan *et al.* used a 100 megaframes per second camera in streak mode to predict bubble-oscillating behavior.<sup>22</sup> More recently, May *et al.* performed high-speed optical experiments on microbubbles with an outer lipid layer, an oil layer, and a gas core.<sup>23</sup> Such microbubbles may have a future application in chemotherapy.<sup>24</sup> The behavior of contrast agent microbubbles near cells has also been under investigation.<sup>25,26</sup> Tachibana *et al.* subjected cells in the presence of a photosensitive drug to continuous ultrasound, and noted surface pores on the cells.<sup>27</sup> What causes this so-called sonoporation is yet unknown, but of great interest for selective delivery of drugs and genes to cells. Recent publications suggest that, even at relatively low acoustic pressures, oscillating microbubbles induce enough shear for the cell membrane to rupture.<sup>28</sup> Okada *et al.* demonstrated cell deformation by microbubbles making use of high-speed photography and fluorescence microscopy.<sup>29</sup> The pore size in the cell membrane has been found to depend on the acoustic pressure.<sup>30</sup>

In the experimental echocardiography laboratory at Erasmus MC, we captured images of insonified medical microbubbles at higher frame rates than the ultrasonic frequency  $T_x$  transmitted (typically  $T_x=0.5$  MHz). We made use of a fast framing camera with a beam splitter, capturing 8 frames at 3 million frames per second, and of the so-called Brandaris-128 rotating mirror camera system, capturing 128 frames at frame rates of 9–13 million frames per

second.<sup>31</sup> Contrast agents were inserted through an artificial capillary with a 200  $\mu\text{m}$  diameter. The artificial capillary was positioned in a container in the acoustical focus of a single-element transducer, and in the optical focus of a high-numerical aperture microscopic system. An overview hereof was more extensively described in Ref. <sup>32</sup>. The potential clinical applications of insonifying medical microbubbles have been explored, based on more than 1,000 high-speed optical image sequences, combined with bubble-sound theory. At low acoustic amplitudes (mechanical index  $\lesssim 0.1$ ) microbubbles pulsate moderately, at high amplitudes (mechanical index  $\gtrsim 0.6$ ) their elongated expansion phase is followed by a violent collapse. In this acoustic regime, microbubbles have been observed to coalesce (merge), fragment, crack, and jet during one single ultrasonic cycle.<sup>32</sup>

The jetting phenomenon for cavitation bubbles can be described as follows.<sup>33</sup> Let's define an infinite boundary at the right of a bubble. During ultrasound insonification, at the moment of maximal expansion (*cf.* Figure 1B1), the pressure inside the bubble is much lower than the ambient pressure, causing the bubble to collapse. The radial water flow is retarded by the boundary. Therefore, the pressure at the right bubble wall is less than the pressure at the right wall during the whole collapse phase and the bubble becomes elongated perpendicular to the boundary. The pressure gradient leads to different accelerations of the left and right bubble walls and therefore to a movement of the center of the bubble towards the boundary during collapse. As the bubble collapses, the fluid volume to the left of the bubble is accelerated and focused leading to the formation of a liquid jet directed towards the boundary. This jet hits the right bubble wall, causing a funnel-shaped protrusion (*cf.* Figure 1B2) and finally impacts the boundary. Empirical relations between bubble radius, jet length, and pressure at the tip of jets have been published in Refs.<sup>34-36</sup> When administering microbubbles in the bloodstream, vessel walls are the boundaries to which ultrasound-induced jets are targeted. An example of microjetting is demonstrated in Figure 1A. Our first observation of microbubble jetting was published in Ref.<sup>37</sup> From our observations of microjetting through medical microbubbles, we

computed that the pressure at the tip of the jet is high enough to penetrate any human cell.<sup>32</sup> Therefore, presumably, the jetting phenomenon causes sonoporation. As such, liquid jets might act as microsyringes, delivering a drug to a region of interest.<sup>32</sup>

Since jetting has been associated with rapid collapse, this phenomenon is not expected with thick-shelled microbubbles, whose oscillation amplitudes are only a few percent of their radii. Although these hard-shelled microbubbles would seem to be unsuitable for therapeutic purposes, they demonstrate the sonic cracking phenomenon at relatively high MI. Sonic cracking is the ultrasound-induced formation of a nanoshell defect causing gas to escape from encapsulated microbubbles.<sup>17</sup> Figure 2 demonstrates that the ultrasound-induced release of gas from an encapsulated microbubble is feasible: Using a peak-negative acoustic pressure of 0.8 MPa at 0.5 MHz, we released gas from albumin-encapsulated microbubbles during an ultrasonic cycle ( $2\ \mu\text{s}$ ).<sup>38</sup> This acoustic pressure is well within in the clinical diagnostic range. Gas is seen to escape from an albumin-encapsulated microbubble with a  $4.3\ \mu\text{m}$  diameter in the third frame, in the beginning of the rarefaction phase of the ultrasound. The nanoshell itself is too rigid to expand. The free gas expands to a diameter of  $12.3\ \mu\text{m}$  in the eighth frame, after which it contracts. In the eleventh frame, the free gas microbubble, which has been subjected to motion blur, appears to be detached from the encapsulated microbubble. In the twelfth frame, the gas is hardly visible, owing to the compression phase of the ultrasound. Medical microbubbles act as the vehicle to carry a drug in the gaseous phase to a region of interest, where it should be subjected to high-intensity ultrasound. Consequently, the gas is released upon which its diffusion begins.

Because the released gas microbubbles do not have an encapsulation, they exhibit large-amplitude oscillations. These bubbles may fragment during the collapse phase, owing to the enormous rise in kinetic energy relative to the surface energy.<sup>39</sup> We have, however, also observed jetting of released gas microbubbles (*cf.* Figure 3). Hence, the jetting phenomenon may be observed with both thin- and thick-shelled ultrasound contrast agents.

We propose to include the nitric oxide (NO) as a gas core of the medical microbubble. In the vasculature, NO is produced by the endothelium and diffuses into the luminal and abluminal regions. NO traveling into smooth muscle initiates a series of reactions that lead to vessel dilation.<sup>40</sup> Targeting NO to areas of early atherosclerosis might also prove to be useful in preventing plaque formation.<sup>41</sup> Due to the high diffusivity of NO, however, the drug has to be applied locally or in large quantities, in order to have the effect desired. Here, ultrasound-induced microbubble-assisted drug delivery may prove to be fruitful. Small quantities of NO microbubbles might be administered, and released at the region of interest by means of sonic cracking. The mean diameter size of released gas microbubbles from thick-shelled contrast agent microbubbles has been measured  $1.5\ \mu\text{m}$ ,<sup>38</sup> which corresponds to a 1.7 femtomol gas content. This is already more than the NO production of a 1 mm long vessel with a  $50\ \mu\text{m}$  diameter during 100 ms.<sup>40</sup>

The complicated behavior of medical microbubbles in high-amplitude ultrasonic fields becomes more and more understood. This opens up a whole new area of potential applications of diagnostic ultrasound related to targeted imaging and therapeutic delivery of drugs such as nitric oxide.

## Acknowledgments

The authors are grateful to Bracco Research SA, Genève, Switzerland, for supplying an experimental contrast agent, and Upperton Limited, Nottingham, UK, for supplying the contrast agent Quantison<sup>TM</sup>. This project has been supported by the Technology Foundation STW (RKG.5104).

## References

- <sup>1</sup> J. R. Lindner, “Microbubbles in medical imaging: current applications and future directions”, *Nature* **3**, 527–532 (2004).
- <sup>2</sup> E. Stride, N. Saffari, “Microbubble ultrasound contrast agents: a review”, *Proc. Instn Mech. Engrs* **217**, 429–447 (2003).
- <sup>3</sup> H. Heynemann, K.-V. Jenderka, M. Zacharias, P. Fornara, “Neue Techniken der Urosonographie”, *Urologe* **43**, 1362–1370 (2004).
- <sup>4</sup> P. Heppner, J. R. Lindner, “Contrast ultrasound assesment of angiogenesis by perfusion and molecular imaging”, *Expert Rev. Mol. Diagn.* **5**, 447–455 (2005).
- <sup>5</sup> R. V. Shohet, S. Chen, Y. T. Zhou, Z. Wang, R. S. Meidell, R. H. Unger, P. A. Grayburn, “Echocardiographic destruction of albumin microbubbles directs gene delivery to the myocardium”, *Circulation* **101**, 2554–2556 (2000).
- <sup>6</sup> E. C. Unger, T. O. Matsunaga, T. McCreery, P. Schumann, R. Sweitzer, R. Quigley, “Therapeutic applications of microbubbles”, *Eur. J. Radiol.* **42**, 160–168 (2002).
- <sup>7</sup> Y. Taniyama, K. Tachibana, K. Hiraoka, T. Namba, K. Yamasaki, N. Hashiya, M. Aoki, T. Ogihara, K. Yasufumi, R. Morishita, “Local delivery of plasmid DNA into rat carotid artery using ultrasound”, *Circulation* **105**, 1233–1239 (2002).
- <sup>8</sup> L. L. Endelman, “A brief history of high speed photography 1851–1930”, Presented at: SPIE 32nd Annu. Int. Tech. Symp. (1988).
- <sup>9</sup> E. Mach, P. Salcher, “Photographische Fixirung der durch Projectile in der Luft eingeleiteten Vorgänge”, *Sitzungsberichte d. kais. Akad. d. Wiss. mathem.-naturw. Classe* **95**, 764–780 (1887).

- <sup>10</sup> C. V. Boys, “On electric spark photographs; or, photography of flying bullets, etc., by the light of the electric spark”, *Nature* **47**, 415–421 (1893).
- <sup>11</sup> A. M. Worthington, R. S. Cole, “Impact with a liquid surface studied by the aid of instantaneous photography. Paper I”, *Philos. Trans. Roy. Soc. A* **189**, 137–149 (1897).
- <sup>12</sup> P. W. W. Fuller, J. T. Rendell, “The development of high speed photography”, in “High speed photography and photonics”, , edited by S.F. Ray (SPIE, Washington, 2002), 7–28.
- <sup>13</sup> A. L. Klibanov, K. W. Ferrara, M. S. Hughes, J. H. Wible Jr., J. K. Wojdyla, P. A. Dayton, K. E. Morgan, G. H. Brandenburger, “Direct video-microscopic observation of the dynamic effects of medical ultrasound on ultrasound contrast microspheres”, *Invest. Radiol.* **33**, 863–870 (1998).
- <sup>14</sup> P. Dayton, K. Morgan, M. Allietta, A. Klibanov, G. Brandenburger, K. Ferrara, “Simultaneous optical and acoustical observations of contrast agents”, *Proc. IEEE Ultrason. Symp.* 1583–1591 (1997).
- <sup>15</sup> P. A. Dayton, K. E. Morgan, A. L. Klibanov, G. H. Brandenburger, K. W. Ferrara, “Optical and acoustical observations of the effects of ultrasound on contrast agents”, *IEEE Trans. Ultrason., Ferroelect., Freq. Contr.* **46**, 220–232 (1999).
- <sup>16</sup> Y. Takeuchi, “Pulsed stroboscopic visualizer to synchronously monitor the microballoon under insonification”, *Proc. IEEE Ultrason. Symp.* 1645–1649 (1998).
- <sup>17</sup> Y. Takeuchi, *IEEE Trans. Ultrason., Ferroelect., Freq. Contr.* **46**, cover (1999).
- <sup>18</sup> M. Postema, A. Bouakaz, C. T. Chin, N. de Jong, “Optically observed microbubble coalescence and collapse”, *Proc. IEEE Ultrason. Symp.* 1900–1903 (2002).
- <sup>19</sup> S. H. Bloch, M. Wan, P. A. Dayton, K. W. Ferrara, “Optical observation of lipid- and polymer-shelled ultrasound microbubble contrast agents”, *Appl. Phys. Lett.* **84**, 631–633 (2004).

- <sup>20</sup> K. Kuribayashi, N. Kudo, M. Natori, K. Yamamoto, “A high-magnification and high-speed system for the observation of microbubbles under ultrasound exposure”, *Proc. IEEE Ultrason. Symp.* 1755–1758 (1999).
- <sup>21</sup> N. de Jong, P. J. A. Frinking, A. Bouakaz, M. Goorden, T. Schuurmans, X. Jingping, F. Mastik, “Optical imaging of contrast agent microbubbles in an ultrasound field with a 100-MHz camera”, *Ultrasound Med. Biol.* **26**, 487–492 (2000).
- <sup>22</sup> K. E. Morgan, J. S. Allen, J. E. Chomas, P. A. Dayton, K. W. Ferrara, “Experimental and theoretical analysis of individual contrast agent behavior”, *Proc. IEEE Ultrason. Symp.* 1685–1688 (1999).
- <sup>23</sup> D. May, J. Allen, K. Ferrara, “Dynamics and fragmentation of thick-shelled microbubbles”, *IEEE Trans. Ultrason., Ferroelect., Freq. Contr.* **49**, 1400–1410 (2002).
- <sup>24</sup> M. J. Shortencarier, P. A. Dayton, S. H. Bloch, P. A. Schumann, T. O. Matsunaga, K. W. Ferrara, “A method for radiation-force localized drug delivery using gas-filled lipospheres”, *IEEE Trans. Ultrason., Ferroelect., Freq. Contr.* **51**, 822–831 (2004).
- <sup>25</sup> N. Kudo, T. Miyaoka, K. Okada, K. Yamamoto, K. Niwa, “Study on mechanism of cell damage caused by microbubbles exposed to ultrasound”, *Proc. IEEE Ultrason. Symp.* 1351–1354 (2002).
- <sup>26</sup> B. Wolfrum, R. Mettin, T. Kurz, W. Lauterborn, “Observations of pressure-wave-excited contrast agent bubbles in the vicinity of cells”, *Appl. Phys. Lett.* **81**, 5060–5062 (2002).
- <sup>27</sup> K. Tachibana, T. Uchida, K. Ogawa, N. Yamashita, K. Tamura, “Induction of cell-membrane porosity by ultrasound”, *Lancet* **353**, 1409 (1999).
- <sup>28</sup> P. Marmottant, S. Hilgenfeldt, “Controlled vesicle deformation and lysis by single oscillating bubbles”, *Nature* **423**, 153–156 (2003).

- <sup>29</sup> K. Okada, N. Kudo, K. Niwa, K. Yamamoto, “A basic study on sonoporation with microbubbles exposed to pulsed ultrasound”, *J. Med. Ultrasonics* **32**, 3–11 (2005).
- <sup>30</sup> R. Karshafian, S. Samac, M. Banerjee, P. D. Bevan, P. N. Burns, “Ultrasound-induced uptake of different size markers in mammalian cells”, *Abstr. IEEE Ultrason. Symp.* 145–146 (2005).
- <sup>31</sup> C. T. Chin, C. Lancée, J. Borsboom, F. Mastik, M. Frijlink, N. de Jong, M. Versluis, D. Lohse, “Brandaris 128: a 25 million frames per second digital camera with 128 highly sensitive frames”, *Rev. Sci. Instru.* **74**, 5026–5034 (2003).
- <sup>32</sup> M. Postema, A. van Wamel, C. T. Lancée, N. de Jong, “Ultrasound-induced encapsulated microbubble phenomena”, *Ultrasound Med. Biol.* **30**, 827–840 (2004).
- <sup>33</sup> A. Philipp, W. Lauterborn, “Cavitation erosion by single laser-produced bubbles”, *J. Fluid Mech.* **361**, 75–116 (1998).
- <sup>34</sup> T. Kodama, K. Takayama, “Dynamic behavior of bubbles during extracorporeal shock-wave lithotripsy”, *Ultrasound Med. Biol.* **24**, 723–738 (1998).
- <sup>35</sup> C. D. Ohl, R. Ikink, “Shock-wave-induced jetting of micron-size bubbles”, *Phys. Rev. Lett.* **90**, 214502 (2003).
- <sup>36</sup> C. D. Ohl, E. Ory, “Aspherical bubble collapse — comparison with simulations”, in “Nonlinear Acoustics at the Turn of the Millennium”, , edited by W. Lauterborn, T. Kurz (American Institute of Physics, New York, 2000), 393–396.
- <sup>37</sup> M. Postema, A. Bouakaz, N. de Jong, *IEEE Trans. Ultrason., Ferroelect., Freq. Contr.* **49(3)**, cover (2002).
- <sup>38</sup> M. Postema, A. Bouakaz, M. Versluis, N. de Jong, “Ultrasound-induced gas release from contrast agent microbubbles”, *IEEE Trans. Ultrason., Ferroelect., Freq. Contr.* **52**, 1035–1041 (2005).

- <sup>39</sup> M. Postema, G. Schmitz, “Ultrasonic fragmentation of microbubbles: a theoretical approach of the flash in flash-echo”, Proc. IEEE Eng. Med. Biol. Soc. **#33** (2005).
- <sup>40</sup> M. W. Vaughn, L. Kuo, J. C. Liao, “Estimation of nitric oxide production and reaction rates in tissue by use of a mathematical model”, Am. J. Physiol. **274**, H2163–H2176 (1998).
- <sup>41</sup> I. L. Megson, “Nitric oxide donor drugs”, Drugs Fut. **25**, 701–715 (2000).

## List of Figures

- 1 Two high-speed photographic frames (A1,2) and an overlaid image thereof (A3) of microjetting — a microbubble acting as a microsyringe — and a schematic representation of this phenomenon (B). On the verge of microjetting (1, thin line), the microbubble has a diameter of  $17\ \mu\text{m}$ . During microjetting (2), liquid protrudes through the right side of the microbubble, over a length of  $l = 26\ \mu\text{m}$ . The jet is represented by the bold curve. The time between the two frames is  $0.33\ \mu\text{s}$ . . . . . 14
- 2 Gas release from the upper left of a nanoshelled microbubble during a single ultrasonic cycle (A), and a schematic representation thereof (B). During the rarefaction phase (starting frame 2), gas escapes until it reaches a maximum (frame 8). During the subsequent contraction, the free gas bubble is seen detached from the nanoshell (frames 11 and 12). Each frame corresponds to a  $19 \times 19\ \mu\text{m}^2$  area. The interframe times are  $0.1\ \mu\text{s}$ . © 2005 IEEE. Modified and printed with permission from M. Postema, A. Bouakaz, M. Versluis, N. de Jong, “Ultrasound-induced gas release from contrast agent microbubbles”, IEEE Trans. Ultrason., Ferroelect., Freq. Contr. **52**, 1035–1041 (2005). . . . . 15

- 3 Gas release and jetting of the released gas bubble. Frame a has been taken prior to ultrasound arrival. Gas escaping from the shell is clearly visible in frame b, which has been captured  $2.2 \mu s$  after frame a. The gas has detached from the shell in frame 1, taken  $0.9 \mu s$  after frame b. During the rarefaction phase, the escaped gas expands to twice the encapsulation radius. During collapse, in frame 9, a jet towards the left is visible. On rebound, in frame 10, the free gas bubble still demonstrates spherical asymmetry. Frames 1–10 were captured during insonification with 8 cycles of  $T_x=1.7$  MHz ultrasound with a peak rarefactional acoustic pressure of  $p^- = 1.5$  MPa. Each frame corresponds to a  $25 \times 11 \mu m^2$  area. The interframe times of frames 1–10 are  $0.08 \mu s$ . . . . . 16

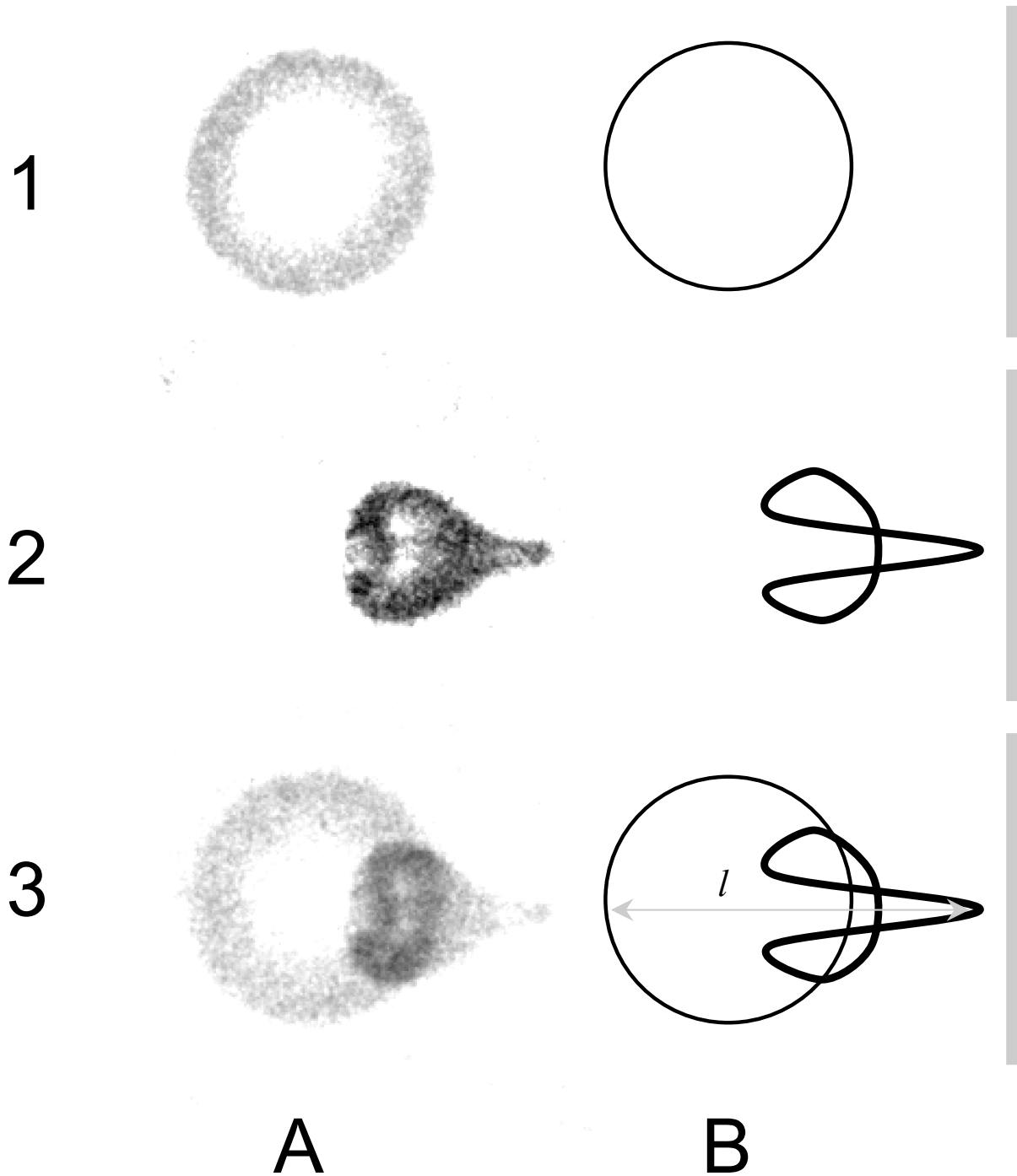
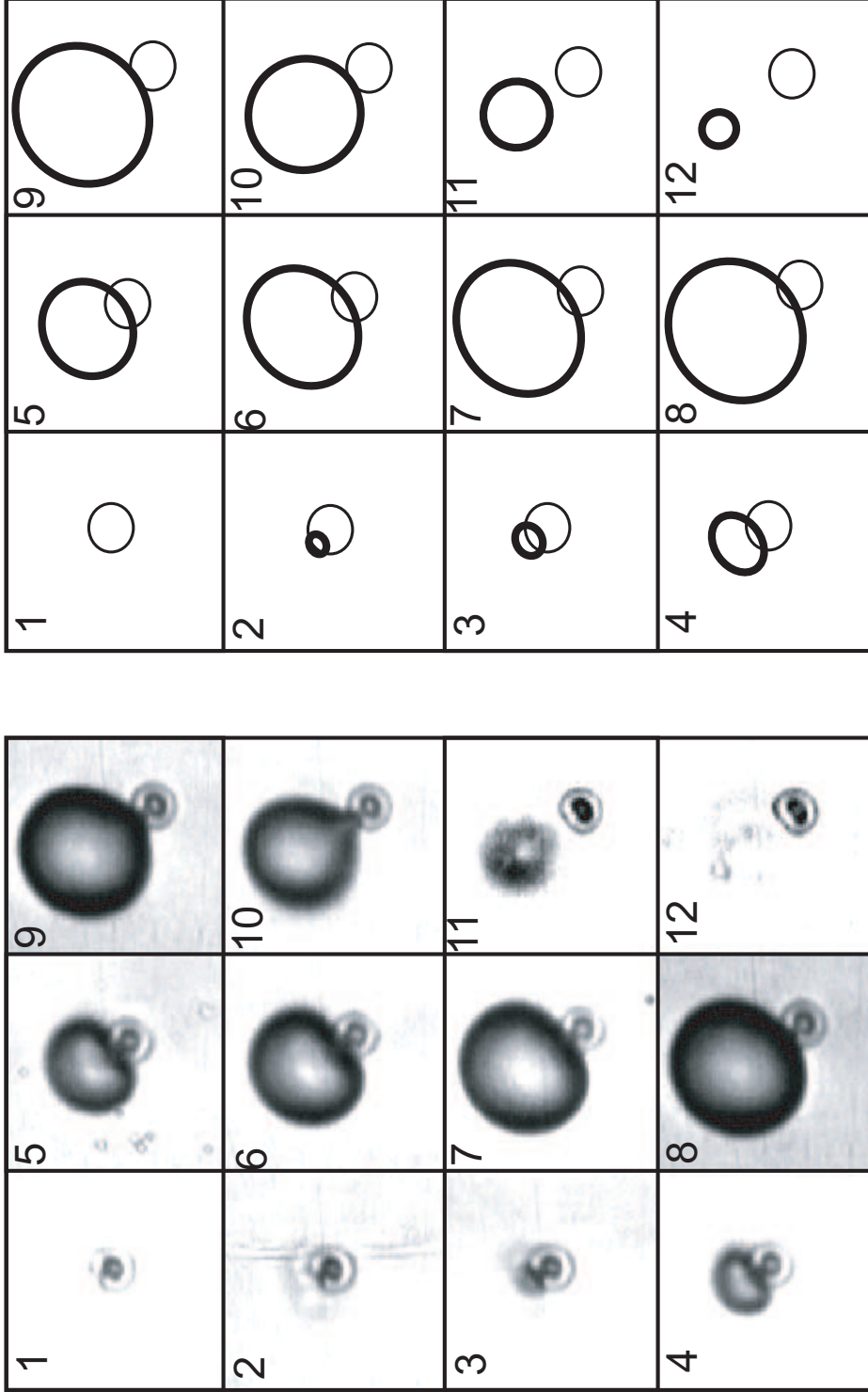


Figure 1: Two high-speed photographic frames (A1,2) and an overlaid image thereof (A3) of microjetting — a microbubble acting as a microsyringe — and a schematic representation of this phenomenon (B). On the verge of microjetting (1, thin line), the microbubble has a diameter of  $17\ \mu\text{m}$ . During microjetting (2), liquid protrudes through the right side of the microbubble, over a length of  $l = 26\ \mu\text{m}$ . The jet is represented by the bold curve. The time between the two frames is  $0.33\ \mu\text{s}$ .



**A**

**B**

Figure 2: Gas release from the upper left of a nanoshelled microbubble during a single ultrasonic cycle (A), and a schematic representation thereof (B). During the rarefaction phase (starting frame 2), gas escapes until it reaches a maximum (frame 8). During the subsequent contraction, the free gas bubble is seen detached from the nanoshell (frames 11 and 12). Each frame corresponds to a  $19 \times 19 \mu\text{m}^2$  area. The interframe times are  $0.1 \mu\text{s}$ . © 2005 IEEE. Modified and printed with permission from M. Postema, A. Bouakaz, M. Versluis, N. de Jong, "Ultrasound-induced gas release from contrast agent microbubbles", IEEE Trans. Ultrason., Ferroelect., Freq. Contr. **52**, 1035–1041 (2005).

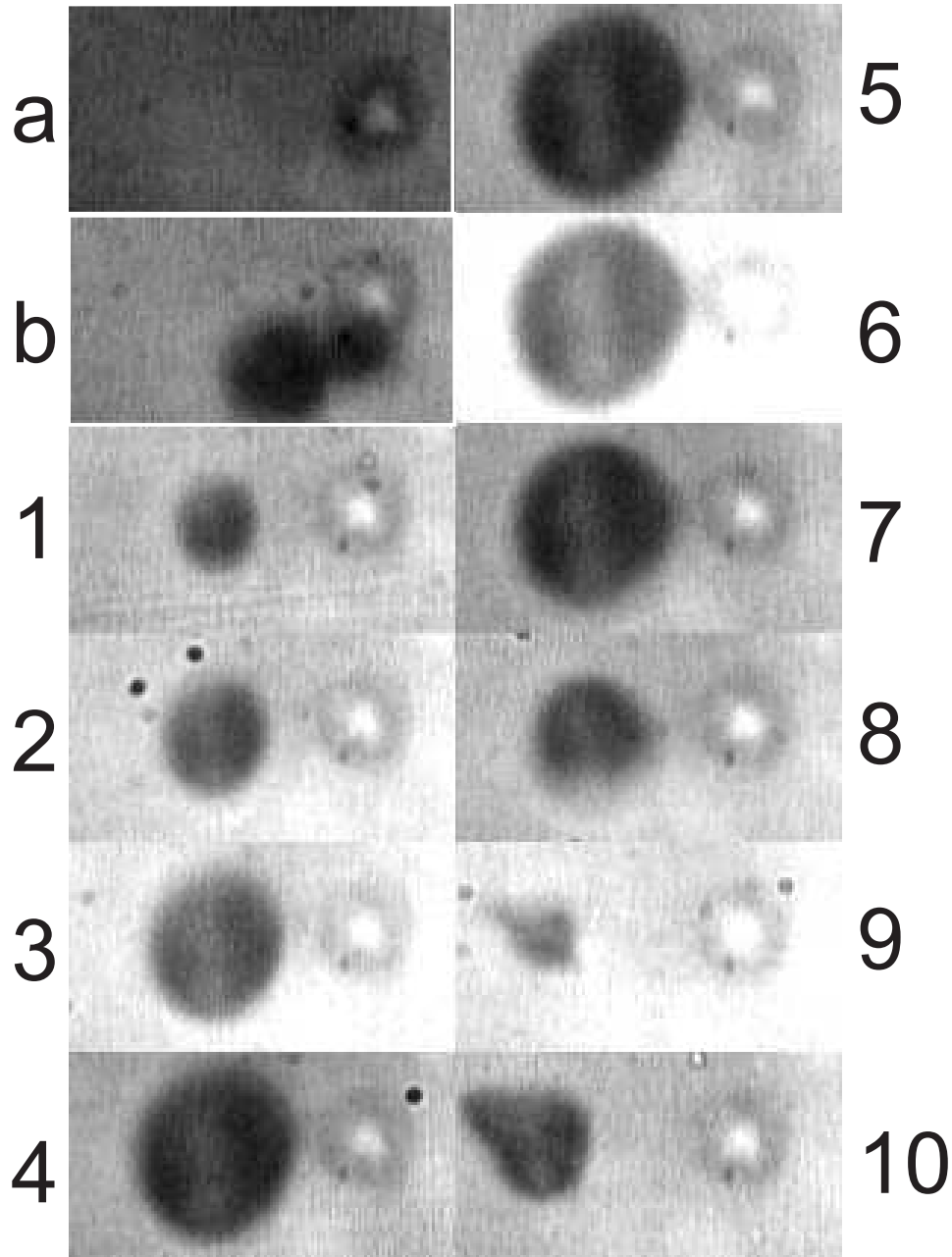


Figure 3: Gas release and jetting of the released gas bubble. Frame a has been taken prior to ultrasound arrival. Gas escaping from the shell is clearly visible in frame b, which has been captured  $2.2 \mu\text{s}$  after frame a. The gas has detached from the shell in frame 1, taken  $0.9 \mu\text{s}$  after frame b. During the rarefaction phase, the escaped gas expands to twice the encapsulation radius. During collapse, in frame 9, a jet towards the left is visible. On rebound, in frame 10, the free gas bubble still demonstrates spherical asymmetry. Frames 1–10 were captured during insonification with 8 cycles of  $T_x=1.7$  MHz ultrasound with a peak rarefactional acoustic pressure of  $p^- = 1.5$  MPa. Each frame corresponds to a  $25 \times 11 \mu\text{m}^2$  area. The interframe times of frames 1–10 are  $0.08 \mu\text{s}$ .